Lab on a Chip

Miniaturisation for chemistry, physics, biology, & bioengineering

www.rsc.org/loc

Volume 9 | Number 18 | 21 September 2009 | Pages 2613–2744

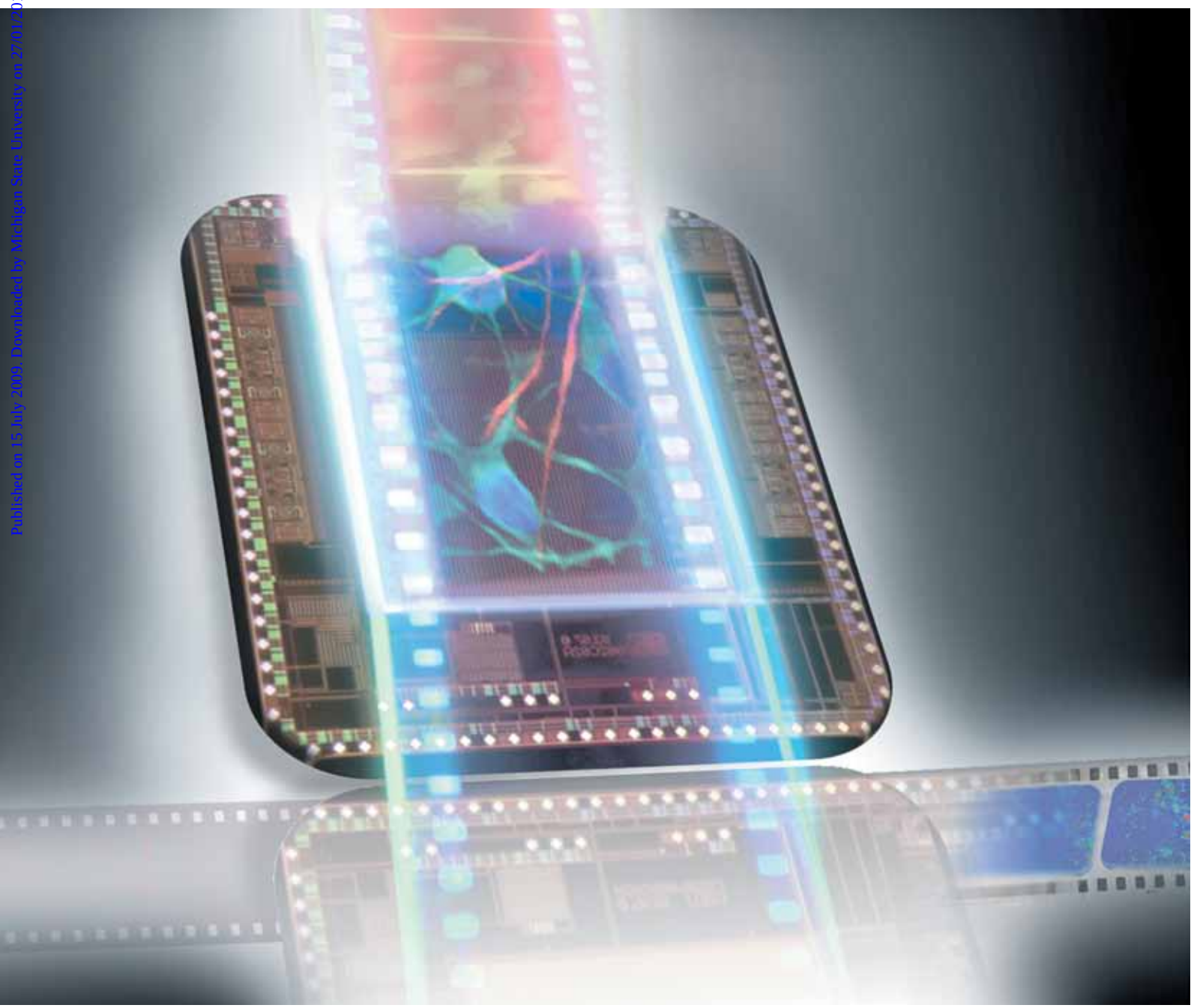

ISSN 1473-0197

RSC Publishing

Active pixel sensor array for high spatio-temporal resolution electrophysiological recordings from single cell to large scale neuronal networks†

Luca Berdondini,*[a] Kilian Imfeld,[b] Alessandro Maccione,[a] Mariateresa Tedesco,[c] Simon Neukom,[d] Milena Koudelka-Hep[b] and Sergio Martinoia[ac]

Received 14th April 2009, Accepted 1st July 2009
First published as an Advance Article on the web 15th July 2009
DOI: 10.1039/b907394a

This paper presents a chip-based electrophysiological platform enabling the study of micro- and macro-circuitry in *in-vitro* neuronal preparations. The approach is based on a 64 × 64 microelectrode array device providing extracellular electrophysiological activity recordings with high spatial (21 μm of electrode separation) and temporal resolution (from 0.13 ms for 4096 microelectrodes down to 8 μs for 64 microelectrodes). Applied to *in-vitro* neuronal preparations, we show how this approach enables neuronal signals to be acquired for investigating neuronal activity from single cells and microcircuits to large scale neuronal networks. The main elements of the platform are the metallic microelectrode array (MEA) implemented in Complementary Metal Oxide Semiconductor (CMOS) technology similar to a light imager, the in-pixel integrated low-noise amplifiers (11 μV_{rms}) and the high-speed random addressing logic. The chip is combined with a real-time acquisition system providing the capability to record at 7.8 kHz/electrode the whole array and to process the acquired signals.

Introduction

One of the central concepts of contemporary neuroscience is that major brain functions are executed through the joint actions of neurons. Individual elements of information are encoded not by single cells, but rather by a population of cells and/or dynamically instantiated cell assemblies.[1] The interplay between single cells, small cell networks (*i.e.* microcircuits) and large population cell assemblies is still largely unknown.[2] In order to bridge the gap between single or multiple cell electrophysiology[3] and neuronal population electrophysiology[4] new enabling technologies are needed both for *in-vitro* and *in-vivo* experiments.[5]

In this context microelectrode arrays (MEAs) represent a valuable experimental tool and are therefore increasingly used for neuroscientific studies, integrated on planar substrates for *in-vitro* research[6,7] or on shaped substrates adapted to *in-vivo* implantation.[8,9] *In-vitro*, MEAs are used either on dissociated neuronal preparations[10] or on brain slices[11] and several works explored the potential use of MEA-based platforms for drug-screening and biosensing.[12–16]

Commercially available (*e.g.* Multi Channel Systems, Reutlingen, Germany; Panasonic, Osaka, Japan; Ayanda Biosystems, Lausanne, Switzerland) and constantly improved during the last thirty years, MEAs are the subject of several microtechnology developments.[17] Efforts were oriented at improving the recording and stimulation performances by modifying the electrode materials, *e.g.* TiN, Pt, Au, IrOx, Black-Pt and recently CNTs,[18–20] and the electrode morphologies, *e.g.* planar, neurocages[21] or tip-shaped.[22,23] By taking advantage of the key features of MEAs, *i.e.* long-term recording and bi-directional interfacing, other advancements were focused on completing the functional features of MEA. This includes the integration of physical and chemical sensors,[24] microstructures for network patterning[25–28] and microfluidics.[29,30] Very recently, the recording capabilities of MEAs were extended to the acquisition of axonal signals by integrating PDMS microtunnels to guide and isolate axonal growth.[31]

Even though the increasing impact and relevant contributions aimed at upgrading MEA-based devices, the potentialities of this approach to map neuronal signalling in large-scale networks at spatial resolution down to cellular resolutions are still not available. This improvement requires innovative approaches to integrate large and dense microelectrode arrays and to read-out signals at sufficient temporal resolution to perform spike detection and data analysis (*e.g.* > 6 kHz). Indeed, currently available devices based on thin-film technology are limited both in spatial resolution (typically 100 μm) and in the number of integrated

[a]*Neuroscience and Brain Technologies, Italian Institute of Technology, Via Morego 30, 16163 Genova, Italy; Fax: +39 010 720321; Tel: +39 010 71781520. E-mail: Luca.Berdondini@iit.it*
[b]*Institute of Microtechnology, EPFL-STI-IMT NE, Rue Jaquet-Droz 1, 2007 Neuchatel, Switzerland. E-mail: Imt-ne-samlab@epfl.ch; Fax: +41 32 7205 711; Tel: +41 32 7205 121*
[c]*Department of Biophysical and Electronic Engineering, University of Genova, Via All'Opera Pia, 16145 Genova, Italy. E-mail: Sergio.Martinoia@unige.it; Fax: +39 010 3532133; Tel: +39 010 3532251*
[d]*Centre Suisse d'Electronique et de Microtechnique SA, Technoparkstrasse 1, 8005 Zürich, Switzerland. E-mail: Simon.Neukom@csem.ch; Fax: +41 44 497 1400; Tel: +4144 4971411*

† Electronic supplementary information (ESI) available: Neuronal activity movies of the electrophysiological extracellular signals acquired at high resolution and on conventional MEAs. Neuronal signals are visualized in a false colour map by computing the signal variance on a sliding window of 150 frames (samples) recorded at full speed (7.8 kHz). The logarithmic colour scale ranges from 0 (blue) to 600 μV (red). (S1.A) Burst onset at the whole array. (S1.B) and (S1.C) show two sequential burst events with different initiation sites and propagation patterns. (S1.D) Burst onset as recorded by a standard MEA (60 channels, Multichannelsystems). See DOI: 10.1039/b907394a

microelectrodes (range of hundreds) due to the external wiring, and to the amplification and signal conditioning circuitry. With current technology, high resolution measurements are only possible from small active areas.[32]

Our work is aimed at overcoming current spatial–temporal resolution limitations and at validating the developed system in the *in-vitro* field. Thus, we have developed a platform based on monolithic Complementary Metal Oxide Semiconductor technology enabling acquisitions from 4096 microelectrodes at a full frame rate of 7.8 kHz and at a spatial resolution of 21 μm (electrode separation). Based on the Active Pixel Sensor concept (APS), the platform development, electrical characterization and preliminary validation was performed on cardiac tissue.[33] Here, we show the last APS–MEA chip generation and the results achieved on cultured neuronal tissue. To introduce the platform, Fig. 1 presents a schematic description. Briefly, the two essential elements are: (i) the metallic microelectrode array implemented similarly to a light imager, with in-pixel integrated microelectrodes and low-noise amplifiers (11 μV_{rms}); and (ii) a real-time acquisition and processing board. Based on image/video concepts implemented in hardware, the signal and data processing is furthermore adapted for handling a very large data flow (typically 0.5 Gbit/s). The platform enables acquisitions with a spatial resolution comparable to mammalian neuronal cell bodies (*i.e.*, microelectrode size and a separation of 21 μm), and a temporal resolution down to 8 μs/pixel on 64 selected pixel-microelectrodes.

Our system outperforms analogous CMOS–MEA devices recently proposed in the literature[34–36] since it allows accessing in real-time the spatial–temporal correlation of activities at both local and network levels acquired from 4096 microelectrodes.

Results and discussion

Experimental work was oriented towards the validation of the platform on neuronal cultures and the presented results have the aim to highlight the potentialities of the platform for neurophysiologic applications. As shown in Fig. 2 the approach relies on a custom microelectrode array integrating high-speed circuitry for acquiring electrophysiological images from which single pixel activity can be extracted and reconstructed in real-time. The chip was fully electrically validated as reported in our previous publication presented by Imfeld *et al.*[33] The last generation used in this work does not change in the overall characteristics, but it is optimized with respect to the stability of the amplification circuitry. The characteristics of the systems are summarized in Table 1.

To validate the developed platform, we used hippocampal cell cultures from rat embryos (*i.e.*, embryonic days: E18) plated at medium-high concentrations (*i.e.* final density of 1000–1500 cells/mm^2) and cultured for a long period of time (up to 35 DIVs). The experimental model was then extensively characterized under spontaneous conditions or chemical stimulation (see Materials and Methods).

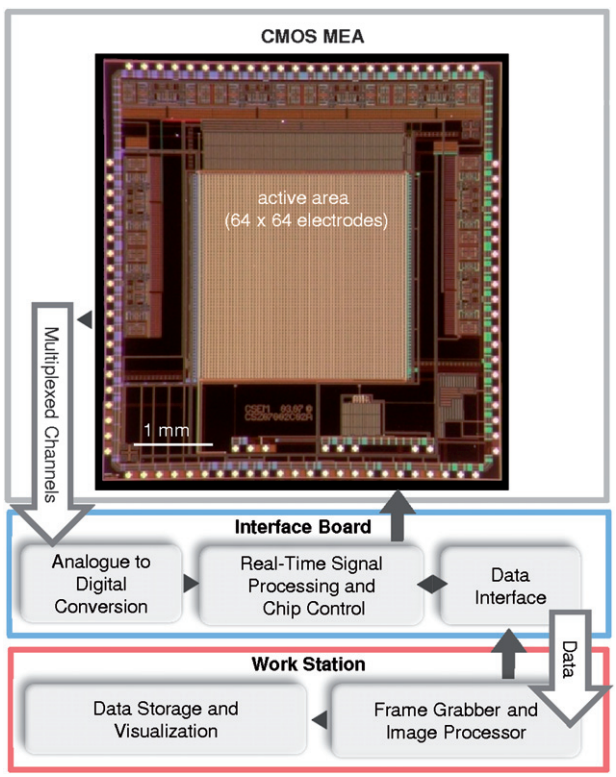

Fig. 1 Overview of the high resolution electrophysiological platform. The system is composed of three hardware levels, *i.e.* the CMOS–MEA chip, the interface board and a work station equipped with a frame grabber for capturing and storing the video stream.

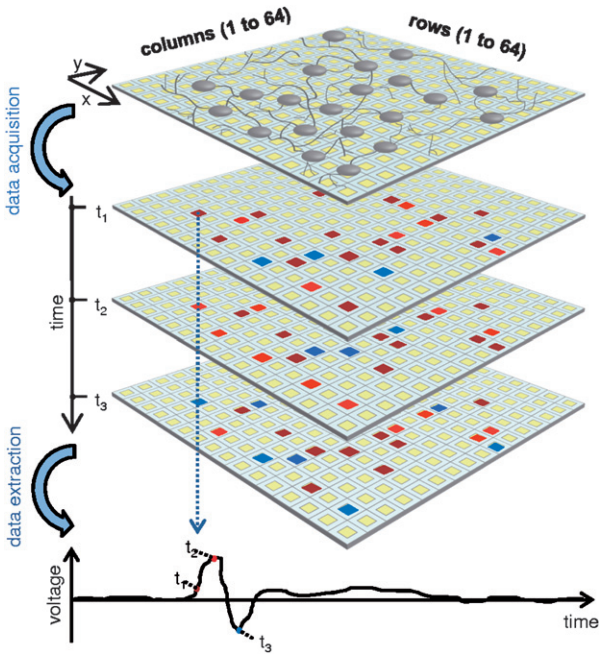

Fig. 2 Working principle of the high resolution platform. Neurons grow and develop chronically on the high-resolution microelectrode array. Fast acquisition of extracellular electrophysiological signals is performed as a sequence of frames by encoding extracellular voltage signals as pixels data. By using a false colour map, this enables the video observation of the overall network activity as well as local activity on the basis of single pixel data. Single microelectrode raw data is reconstructed by combining single pixel data from sequential frames.

Table 1 Summary of the APS–MEA platform characteristics

Number of electrodes	64 × 64
Electrode size	21 μm × 21 μm
Electrode separation	21 μm
Active area	2.67 mm × 2.67 mm
Chip power consumption	132 mW
Input-referred noise	11 μV_{rms}
Minimum sampling rate (4096 electrodes)	7.8 kHz
Maximum sampling rate (64 electrodes)	125 kHz
ADC resolution	12 bits
Data rate	0.5 Gbit/s

Recordings of extracellular activity from *in-vitro* neuronal networks were acquired from 4096 microelectrodes at a sampling rate of 7.8 kHz/channel. Even though APS-MEAs present a higher noise compared to conventional MEA platforms (11 μV_{rms} *vs.* 3–5 μV_{rms}), good signal to noise ratios were observed (typically 5–10 *vs.* 10–15). We explain this result (still under investigation) with the combined contributions of the adhesion layers used to coat the chip surface (see Materials and Methods) and of the embedded configuration of the electrode sites (about 2 μm in depth) contributing to the sealing of neurons on the electrode sites. We do not have access to the in-pixel electrode for impedance measurements, but the result on the SNR is also an indication of much lower electrode impedance with respect to the in-pixel amplifier input impedance (>1 TΩ at 1.1 kHz).

Starting from the second week after plating, hippocampal cultures show a typical fluctuating network firing rate that is characterized by a fast sequence of small bursts (*i.e.*, densely packed spiking activity of 100–300 ms in duration) and silent periods. As previously reported in the literature,[37,38] the electrophysiological activity is strongly synchronized at the network level depending on the experimental conditions and developmental stage. Electrophysiological acquisitions on our platform demonstrate the radically improved spatial resolution compared to conventional microelectrode array methods, which enables the observation of the dynamic patterns expressed by the network with unprecedented detail. This advantage is illustrated in Fig. 3 by the recorded spontaneous electrophysiological activity recruiting up to 2000 microelectrodes. The raster plot shows the collective behaviour of such 2000 microelectrodes highlighting the pronounced barrage of activity observed during characteristic bursting activity (acquisition time length is 10 min.). The typical oscillating and quasi synchronous activity is well represented by the average firing rate (AFR) at whole network level. This

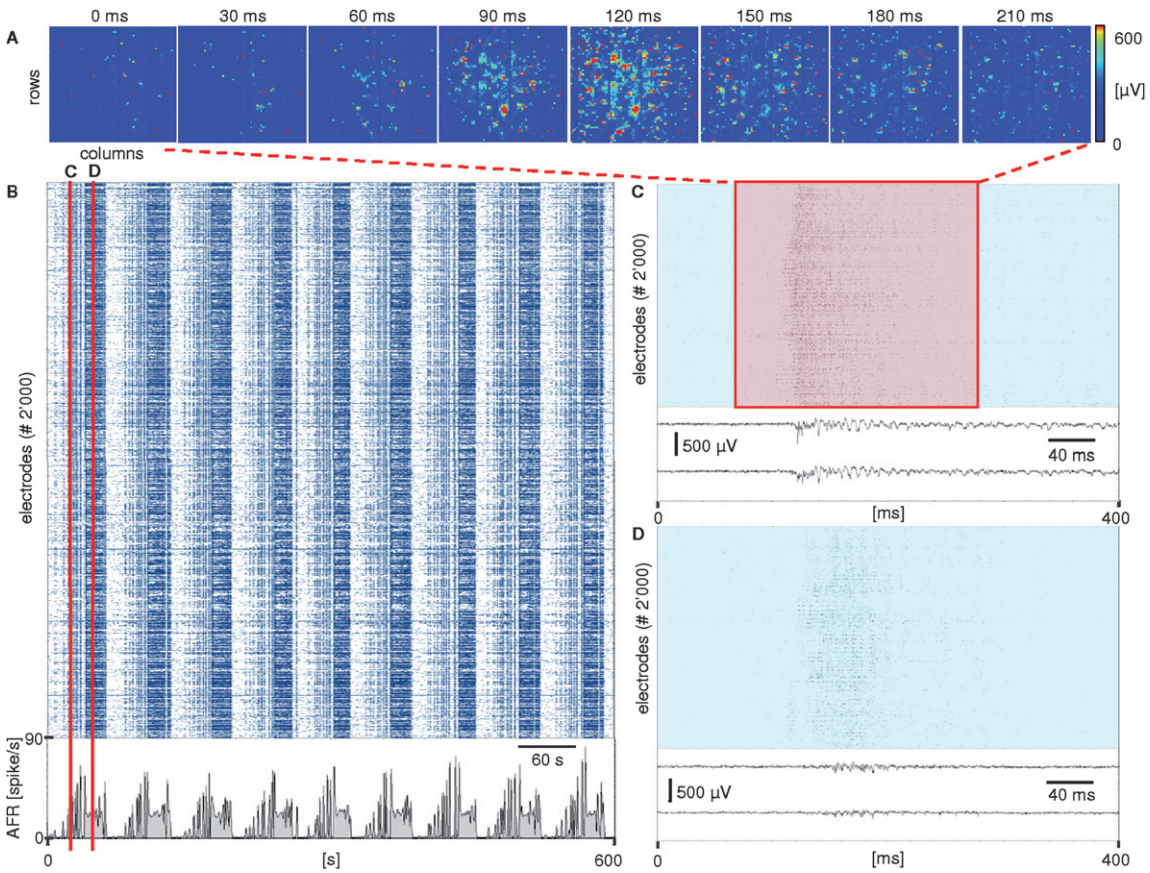

Fig. 3 Spontaneous electrophysiological activity in a dense and mature hippocampal neuronal culture (plating density of 600 cells/μl, 27 DIVs). (A) Single burst activity at global network level represented as an image sequence extracted from the acquired movie (available online as EIS S1.A). The extracellular signals are shown in a false colour map by computing the signal variance (bin size of 20 ms). (B) Raster plot of 2000 active electrode-pixels encompassing several network bursts over a period of 5 min. Bottom panel shows the Average Firing Rate (AFR) demonstrating the quasi-synchronous and oscillating activity at network level. (C, D) Two close-ups of the raster plot, corresponding to two bursts onsets indicated with red lines in (B). Raw data of two exemplificative channels (for both burst onsets) are also presented to appreciate the recorded electrophysiological extracellular signals.

example of acquisition allows appreciating the achieved spatial (Fig. 3, Panel A) and temporal (Fig. 3, Panel C) resolution over thousands of microelectrodes and demonstrates how this method enables to track neuronal signalling and propagation patterns.

The ESI movies S1.A–C† present examples of recordings from hippocampal neuronal cultures at 26–28 DIVs, plated at a fairly high concentration (*i.e.*, final density around 1500 cells/mm^2). Movie S1-A† refers to the bursting activity and frame sequences presented in Fig. 3. Spontaneous activity at the beginning of the burst onset is initiated at a few focused spatial locations and then spread to involve and recruit the large majority of the neurons within the network. Movies S1-B and C† show typical examples of activity patterns (different preparation with respect to Movies S1-A) in which the activity propagates either clockwise or counter clockwise depending on the considered burst. Movies last about 9 s and represent a burst propagation onset of 150 ms. As a reference and comparison, a clip extracted from hippocampal electrophysiological activity recorded with a conventional Micro Electrode Array (MEA, 60 electrodes, 30 μm in diameter, 200 μm spaced, Multichannelsystems), is shown in Movie S1-D.† The poor spatial resolution and the reduced number of electrodes impair any investigation in information transmission properties and propagating activity dynamics. Nevertheless, the mean firing rate calculated on all the microelectrodes that can be considered as active ones (*i.e.*, spike rate >0.1 spikes/s) is in the same range for neuronal cultures of similar densities and ages.

The unique recording resolution of this method also enables the introduction of alternative analysis tools derived from the image processing field for studying neuronal signalling and activations directly on the acquired image sequences (see ESI movie S1.B and S1.C for comparing sequential burst propagations†). A promising method for characterizing neuronal network dynamics at different spatial resolutions, ranging from detailed cellular level to averaged population level, is based on the multi-level spatial wavelet transform applied to the activity images (see also Materials and Methods). In order to follow the initiation and propagation of organized activity, we emphasize the multi-resolution feature of this method by computing the centre of gravity[39] of the wavelet transformed activity at different decomposition levels. Fig. 4 shows the multi-level spatial trajectory for the burst onset for the first 40 ms. The lower spatial resolution (2^{-4}) captures the trajectory of signal propagation at population level while the higher resolution (2^{-1}) enables the propagation at cellular level to be tracked. The method works well if the burst is initiated at a specific location (no multi ignition sites) and it allows also the separation of different activity patterns that could be used for pattern classification. Indeed, in this example three propagation patterns can be easily visually identified showing also the robustness of classification at the different spatial levels.

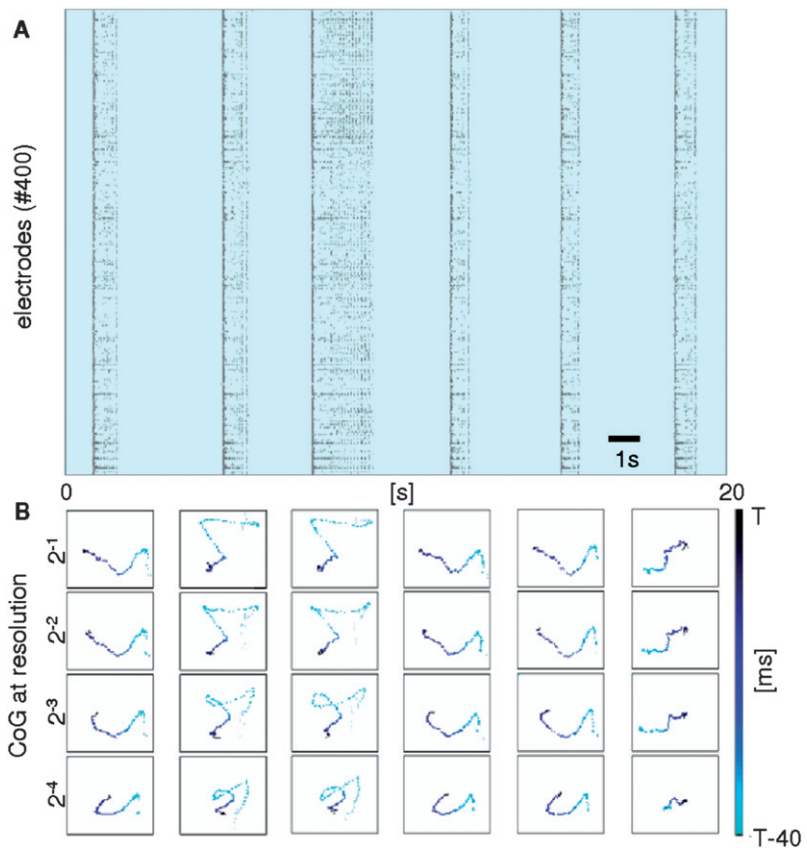

Fig. 4 Characterization of burst dynamics at different spatial resolutions. In this example, the Centre of Gravity (CoGs) of the activity is plotted for the six subsequent bursts shown in raster plot (A). Lower resolutions (*i.e.* 2^{-4}) can monitor the "average" behaviour of a network, whereas higher resolutions (2^{-1}) characterize the network at the cellular level. The trajectories of the CoGs at different resolutions are shown for 40 ms from the onset of each burst (B).

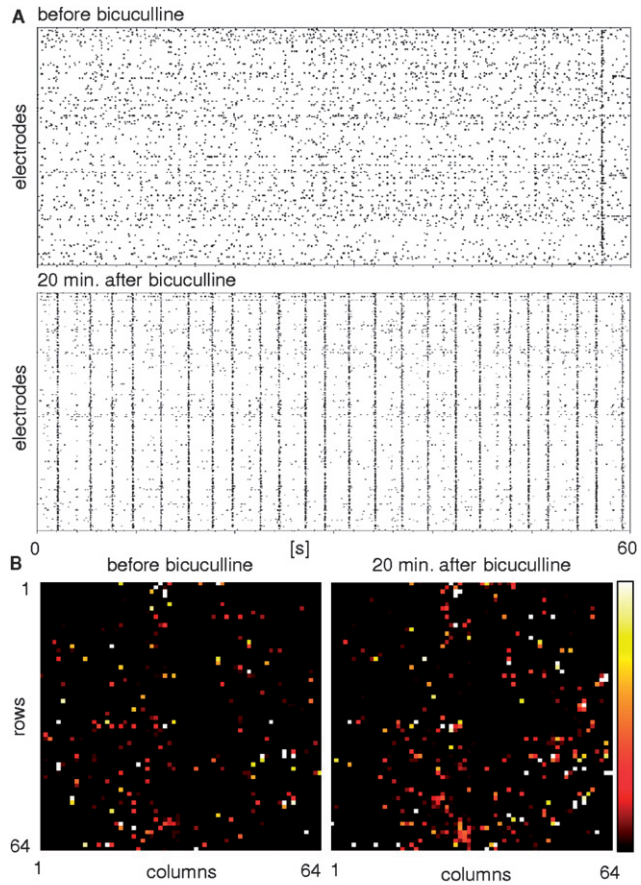

C

	before bicuculline	20 min. after bicuculline
No. Of Valid Channels	251	335
Global MFR [spike/sec]	0,48	0,67
Global Mean ISI [ms]	3754,9	3318,4
Global Bursts	17	29
Global Mean IBI [ms]	3587,9	2600,2
Global Mean Burst Duration [ms]	202,8	149,7
Global Mean IBS [spikes/burst]	5	6

Fig. 5 Example of chemically induced modification of the network activity patterns recorded at high-resolution. Bicuculline (BIC) was applied in the culture media at a concentration of 30 μmol/L and the effects on the network activity (cortical culture at 26 DIVs, final density of 1200 cells/mm^2) are clearly visible comparing the raster plots (A) before and after 20 minutes application of the bicuculline. (B) Representation in false colour maps of the counted spikes for each electrode (black for 0 counts, white for more than 50 spikes) shows that bicuculline increased the number of active channels and extended the involved network area. (C) The summary table reports the main parameters of the chemically induced activity changes. Under bicuculline, the number of spikes and the mean firing rate (MFR) increase, but the inter-spike-interval (ISI), inter-burst-interval (IBI) and mean burst duration are decreased indicating a higher synchrony in the network activity. The intra-burst-spiking rate (IBS) representing the mean number of spikes in a burst, does not significantly change.

Extensive characterization by means of chemical stimulation was also performed to assess our results with similar works performed on conventional MEAs. As an illustrative example, chemically induced activity modifications are shown in Fig. 5. This figure shows two minutes of acquired neuronal signals recorded from a cortical network (DIV26) before and after blocking GABA-A receptors by adding 20 μM bicuculline to the culture media. Raster plots are presented in Fig. 5A. As expected and as widely reported in the literature,[40,41] the network excitability is enhanced and we observe an increased number of active pixels (~34% of increase, Fig. 5B), higher bursting rate and change in the network dynamic profiles (Fig. 5C). The increases in the bursting rates and overall synchrony is indeed not surprising and in perfect agreement with previously presented works. Interestingly enough, the large number of electrodes and high spatial resolution reveal a significant increase in the number of active neurons upon the administration of bicuculline. It is not the aim of this work to enter into a specific neurophysiologic study, but this phenomenon could be systematically studied to further explore the mechanisms of the building of bursting activity in a spontaneously developing neuronal culture.

Relatively dense neuronal cultures limit the imaging capabilities, clear identification of neuronal circuitries and do not ensure single neuron coupling on the electrode sites. In this respect, low-density cultures offer unique opportunities. Indeed, the high-resolution potentialities of the developed system for single neuron measurements are therefore better appreciated on neuronal cultures prepared at lower cell plating densities, thus enabling morphological identification of functional circuits. Fig. 6A shows the image of a region of interest (16 × 16 pixels) of a network at DIV14 obtained by staining the hippocampal cells for neuronal nuclei and dendrites (electrodes visible as black squares). The actual neuronal density is not uniform onto the whole array and is estimated from periphery to centre from 150 to 600 cells/mm^2, respectively. This cell density is in the same range of the pixel-electrode density (570 pixels/mm^2) and approaches thus a one-to-one electrode–neuron correspondence. Fig. 6B shows, as an illustrative example, the related electrophysiological activity acquired by our device (raw data) on three selected neurons possibly participating at a reduced cell assembly or microcircuit. The presented results are preliminary but suggest the finest scale level at which the APS–MEA can be used. In this particular experimental configuration, the combination of immunocytochemical imaging with our high-resolution electrophysiological recording system might be used to investigate, with single neuron resolution, the interplay between architecture and function in neuronal microcircuits (*i.e.*, few interconnected neurons) and large neuronal assemblies (*i.e.*, thousands of cells).

Materials and methods

Chip design and acquisition system

The designed and developed chip enables recording of extracellular potentials on an active area of 2.67 × 2.67 mm^2 at a spatial

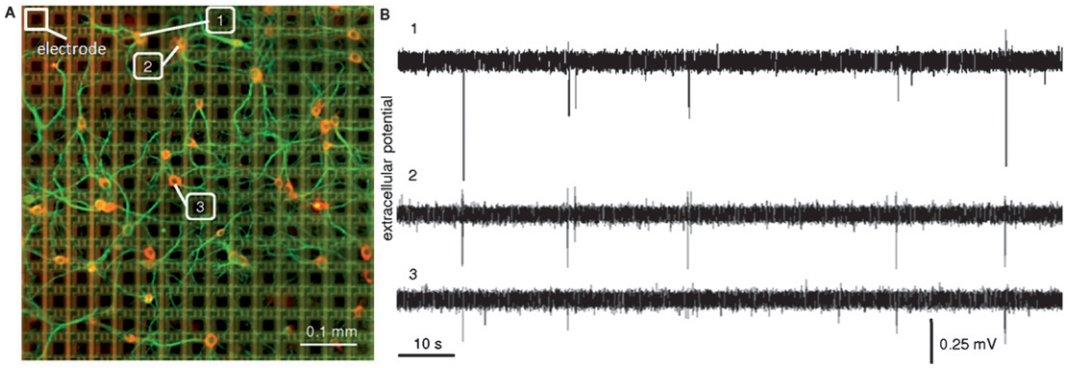

Fig. 6 Combination of high-resolution electrophysiological recording and immunofluorescence imaging enables to resolve single neurons and interconnected microcircuits. (A) Hippocampal network (DIV14) coupled to our device (electrodes visible as black squares under the culture, one electrode is highlighted) and stained with neuN (neuronal cell nuclei – red) and MAP2 (neuronal processes and soma – green); image of a specific region of interest (16 × 16 electrodes). (B) Electrophysiological activity (raw data) of three selected electrodes participating in a small micro-circuit.

resolution (*i.e.*, pitch) of 21 μm and at a sampling frequency of 7.8 kHz/channel for full frame acquisitions and higher frequencies for zoomed acquisitions on Regions of Interest (ROIs). Based on the Active Pixel Sensor (APS) concept originally developed for light imagers, this consisted of implementing into a microelectronic chip (realized in Complementary Metal Oxide Semiconductor – CMOS – technology) an array of 64 × 64 pixels, providing in each pixel a microelectrode of 21 × 21 μm^2 in size and a first amplification stage. On-chip, the pixel outputs are further amplified with an overall gain of 450 and the signals are multiplexed on 16 analogue outputs. Given the dominant effect of the in-pixel circuitry on the noise performances, optimization of the noise level required a trade-off with the pixel size. For a pixel dimension of 42 × 42 μm^2 (electrode area of 21 × 21 μm^2) a static root mean square noise of 11 μV was achieved.

The acquisition system enables raw data to be stored as frame sequences at an average speed of 62 MB/s and provides chip control, high-speed digital addressing, signal acquisition (12 bits resolution) and real-time image/video processing capabilities. These functionalities are provided by a custom platform connected to a commercial frame-grabber (Leonardo PCI64-CL-P-FL-X300-C-128, Arvoo, Woerden, The Netherlands).

Neuronal cell culture and immunocytochemistry

Principles of laboratory animal care of the European Communities Council (86/609/EEC) were followed for the preparation of dissociated neuronal cultures. Primary cultures were obtained from brain tissue of Sprague Dawley rats at embryonic day 18 (E18) using protocols reported in previous works. Briefly, embryos were removed and dissected under sterile conditions. Cortex and hippocampi were dissociated by enzymatic digestion in Trypsin 0.125% –20 min at 37 °C – and finally triturated with a fire-polished Pasteur pipette. Dissociated neurons were plated on the active area of the APS–MEAs, previously coated with poly-D-lysine and laminin. To cover the whole active area of 2.67 × 2.67 mm^2, we used drops of various volumes of cell suspensions from 25 to 40 μl and variable cell concentrations (*i.e.*, from 200 to 2000 cells/μl). The obtained final densities are from about 150 to 1500 cells/mm^2. The different experimental conditions obtained allowed us to explore different network dynamics and to approach the one-to-one correspondence between single neuronal body and pixel in the case of the lower range plating. One hour later, when cells adhered to the substrate, 1 ml of medium was added to each device. The cells were incubated with 1% Glutamax, 2% B-27 supplemented Neurobasal Medium (Invitrogen), in a humidified atmosphere 5% CO_2, 95% air at 37 °C; 50% of the medium was changed every week. No antimitotic drug was used, because application of serum-free medium limits the growth of non-neuronal cells.[42] Hippocampal and cortical neuronal networks were obtained at a final density ranging from 150 to 1200 cells/mm^2. Spontaneous electrical activity recordings were performed starting from the second week of cell culturing.

After the electrophysiological recordings, cells were fixed at room temperature in 4% (w/v) paraformaldehyde in PBS, permeabilized for 10 minutes with 0.1% Triton-X100 and 0.01% Sodium Azide, and exposed for 30–40 minutes to a blocking buffer containing 5% BSA, 0.1% Triton-X100 in PBS. Successively, the cultures were incubated for 2 hours with a mixture of two primary antibodies rabbit polyclonal anti-MAP2 (Chemicon-Millipore AB5622 dilution 1 : 500)[43] and mouse monoclonal anti-NeuN (Chemicon-Millipore MAB 377 dilution 1 : 200) diluted in blocking buffer to reduce nonspecific binding. Then, cells were labelled with the following secondary antibodies: Alexa-Fluor488conjugated goat-antirabbit for MAP2 and Alexa-Fluor 546 conjugated goat-antimouse for NeuN (dilution 1 : 1000).

The antibodies were selected for characterizing the distribution and connection of neurons inside the culture. Immunostaining for MAP2 was used to identify mature neuron dendritic arborizations, whereas immunostaining for NeuN revealed the number of post-mitotic neurons, which start morphological differentiation.

Data analysis

Extracellular electrophysiological neuronal signals were acquired from spontaneously active hippocampal and cortical cultures, at full-frame resolution (7.8 kHz from 4096 electrodes) and for recording phases of 2 to 10 minutes.

During acquisition of electrophysiological neuronal activity, the APS-MEA platform enables observation of signal propagations and neuronal activations. The system processes in-real-time the acquired electrophysiological data as movies by encoding the instantaneous extracellular potential for each electrode in a false colour map. To improve the neuronal signal visualization contrast, the signal variance of each electrode over 20 samples is computed for each frame of the acquired movies. Additionally, single pixel-electrodes can be selected, and raw data can be displayed as a multichannel oscilloscope. Thus, live spatial–temporal neuronal signalling visualization was performed and the acquired movies and raw data were stored for off-line processing.

Single channel raw data were first extracted from the acquisition movies by combining electrode signals of consecutive frames. Then, the single channel raw data were processed with dedicated analysis software integrating previously validated algorithms for processing electrophysiological signals recorded with micro-electrode-arrays (MEA) integrating 60 microelectrodes. A reliable spike detection algorithm was implemented for obtaining high performance temporal accuracy in identifying spiking and bursting events.[44] The spike events were then used for computing global activity parameters by using statistical analysis tools[45,46] as summarized for the example experiment dealing with chemical stimulation (Fig. 5).

The interpretation of data from the high-resolution MEA as a sequence of images opens the door for alternative and complementary analysis methods. While large cultured networks containing thousands of cells can be monitored, the densely integrated electrodes simultaneously allow measuring activity down to the cellular level. This multi-resolution property can also be reflected by appropriate signal processing methods, in particular by wavelet analysis or filter bank theory.[47,48] This concept can be extended to images in order to split and quantify the original information at different resolutions of interest and can be implemented in real-time hardware.[49] We can decompose the activity into a coarse (average) view for global (*i.e.* network) characterization and several higher resolution views to access the activity details down to cell level. To further exploit the multi-resolution capabilities offered by our functional image sequences, we developed *ad-hoc* algorithms for studying at different resolutions the information transmission of the spatial–temporal patterns of bursting events. One of these algorithms includes the computation of trajectories of the Centre of Gravity (CoG) for all approximations A_i ($i = 1 \ldots j$) of the activity down to a low resolution j (Fig. 4).

Conclusions

The aim of this work is to validate our high-resolution recording platform (APS–MEA) for chip integrated electrophysiological studies on neuronal networks and to demonstrate the potentialities enabled by such a high spatial resolution integrated over a large active area.

In particular, we show how the developed APS–MEA device can be used to study synchronous activity, burst initiation and propagation and how efficiently electrophysiological activity at global network level can be investigated, retaining, at the same time, the contributions of smaller networks and the possibility of observing single neuron contribution. Induction of different patterns of activity by means of chemical manipulations, additionally validate the system and illustrate the possibility of using this novel platform to investigate biochemically modified network dynamics, information transmission and processing at high spatial and temporal resolutions.

The APS–MEA platform was designed to handle recordings from the whole active area of 4096 microelectrodes, and in this respect it outperforms other CMOS based systems recently proposed in the literature. Hutzler *et al.*,[36] presented a chip coupled to hippocampal slices constituted by ~16000 electrodes with a separation of 7.8 μm and a full frame rate of 2 kHz. In this case, the image sequence could be acquired, but the main drawbacks rely on poor temporal resolution (spiking activity cannot be resolved) and high noise level (from 50 to 250 μV_{rms}). More recently, Frey *et al.*,[34] proposed a new chip characterized by ~11000 microelectrodes and a very high spatial resolution (3500 electrode/mm^2). However, the architecture of the integrated microelectronic circuit limits the user to select a subset of electrodes (*i.e.*, up to 128) since each selected site is actively wired to a dedicated on-chip amplifier at the beginning of the experiment. This solution enables excellent noise performances to be achieved due to the possibility of integrating the amplifiers on large circuit areas, but hinders the possibility of recording from several thousands of electrodes and to acquire functional movies of propagating signals from the whole network area. Finally, a possible alternative method is represented by the use of voltage sensitive dyes (VSDs). These optical based techniques outperform our approach in terms of spatial resolution (down to sub-cellular level), but current state-of-the-art technology shows slower temporal resolution on similar active areas, worse SNR, and usually shows additional photo-bleaching and photo-toxic effects.[50,51]

The proposed APS–MEA is a trade-off among noise level, spatial resolution and number of recording elements, and offers unique opportunities for studying neuronal dynamics in large populations. Achieved SNRs are comparable with values observed on conventional MEAs and result from the good adhesion and sealing of neurons on the electrode sites. Indeed, these aspects compensate the slightly worst noise performances of our platform introduced by the on-chip multiplexing and non-optimized electrode material resulting from the CMOS processing. This dependency on the cellular adhesion might be reduced by modifying the electrodes with nanomaterials, *e.g.* CNTs, which would increase the real-electrode area, lower the electrode impedance and thus reduce the noise.

The optimization of the electrode material might also improve the re-use of the APS–MEA chips currently limited by electrode degradation. Typically, our devices can be re-used 4–5 times (at 30–40 DIVs per experiment), which is a shorter life-time compared to conventional thin-film fabricated MEAs (tens of times upon appropriate cleaning). In good conditions, APS–MEAs did not show constantly non-working electrodes and only temporal non-functionality of less than 1% of the electrodes was observed. This temporal non-functionality is due to drift effects introduced by pixel mismatch and slightly different electrode behaviours. It is limited to very short durations (maximum of 0.4 ms) since the integrated circuit was designed to constantly calibrate (at 2.5 Hz) the in-pixel amplifiers to reset the working

point. Intensive re-use of the devices tends to increase the amount of non-working electrodes and is our major source of chip failure.

It should be noted that the current implementation does not include in-pixel stimulation in all electrodes. This feature is available only on dedicated electrodes integrated on the sides of the active area (still under testing). The integration of the stimulation feature in all the pixels is indeed an important improvement that will be addressed with the next chip generations. However, implementation of the in-pixel stimulation is a critical issue due to the highly integrated microelectronic circuitry that might be affected by cross-talks between the low-noise recording pathways and the stimulation lines carrying large amplitude stimuli.

In conclusion, the presented high spatial–temporal resolution device, combined with optimized cell culturing and micropatterning techniques, can definitely represent a valuable tool for understanding the formation, significance and dynamical properties of neuronal cell assemblies. As a further exploitation of this approach, the same platform was tested in conjunction with acute slices (data not shown) and we foresee that the same concepts could be integrated on adapted devices for *in-vivo* measurements, thus getting new insights with a functional electrophysiological close-up of brain mapping.

Acknowledgements

This work was supported by a grant from the European Community in the New and Emerging Science and Technology program (IDEA project, FP6-NEST, contract No. 516432).

References

1 M. A. L. Nicolelis, E. E. Fanselow and A. A. Ghazanfar, *Neuron*, 1997, **19**, 219–221.
2 A. K. Engel, P. Fries and W. Singer, *Nat. Rev. Neurosci.*, 2001, **2**, 704–716.
3 G. Q. Bi and M. M. Poo, *Ann. Rev. Neurosci.*, 2001, **24**, 139–166.
4 M. A. L. Nicolelis and S. Ribeiro, *Curr. Opin. Neurobiol.*, 2002, **12**, 602–606.
5 G. Buzsaki, *Nat. Neurosci.*, 2004, **7**, 446–451.
6 G. W. Gross, E. Rieske, G. W. Kreutzberg and A. Meyer, *Neurosci. Lett.*, 1977, **6**, 101–105.
7 J. Pine, *J. Neurosci. Methods*, 1980, **2**, 19–31.
8 G. T. A. Kovacs, C. W. Storment and J. M. Rosen, *IEEE Trans. Biomed. Eng.*, 1992, **39**, 893–902.
9 K. D. Wise, K. Najafi and K. L. Drake, *IEEE Trans. Biomed. Eng.*, 1984, **31**, 583–583.
10 F. O. Morin, Y. Takamura and E. Tamiya, *J. Biosci. Bioeng.*, 2005, **100**, 131–143.
11 U. Egert, D. Heck and A. Aertsen, *Exp. Brain Res.*, 2002, **142**, 268–274.
12 B. D. DeBusschere and G. T. Kovacs, *Biosens. Bioelectron.*, 2001, **16**, 543–556.
13 G. W. Gross, H. M. E. Azzazy, M. C. Wu and B. K. Rhodes, *Biosens. Bioelectron.*, 1995, **10**, 553–567.
14 J. J. Pancrazio, S. A. Gray, Y. S. Shubin, N. Kulagina, D. S. Cuttino, K. M. Shaffer, K. Eisemann, A. Curran, B. Zim, G. W. Gross and T. J. O'Shaughnessy, *Biosens. Bioelectron.*, 2003, **18**, 1339–1347.
15 A. Stett, U. Egert, E. Guenther, F. Hofmann, T. Meyer, W. Nisch and H. Haemmerle, *Anal. Bioanal. Chem.*, 2003, **377**, 486–495.
16 S. Martinoia, L. Bonzano, M. Chiappalone, M. Tedesco, M. Marcoli and G. Maura, *Biosens. Bioelectron.*, 2005, **20**, 2071–2078.
17 T. M. Pearce and J. C. Williams, *Lab Chip*, 2007, **7**, 30–40.
18 E. Ben-Jacob and Y. Hanein, *J. Mat. Chem.*, 2008, **18**, 5181–5186.
19 G. Cellot, E. Cilia, S. Cipollone, V. Rancic, A. Sucapane, S. Giordani, L. Gambazzi, H. Markram, M. Grandolfo, D. Scaini, F. Gelain, L. Casalis, M. Prato, M. Giugliano and L. Ballerini, *Nat. Nanotechnol.*, 2009, **4**, 126–133.
20 E. W. Keefer, B. R. Botterman, M. I. Romero, A. F. Rossi and G. W. Gross, *Nat. Nanotechnol.*, 2008, **3**, 434–439.
21 M. P. Maher, J. Pine, J. Wright and Y.-C. Tai, *J. Neurosci. Methods*, 1999, **87**, 45–56.
22 M. O. Heuschkel, M. Fejtl, M. Raggenbass, D. Bertrand and P. Renaud, *J. Neurosci. Methods*, 2002, **114**, 135–148.
23 P. Thiébaud, N. F. de Rooij, M. Koudelka-Hep and L. Stoppini, *IEEE Trans. Biomed. Eng.*, 1997, **44**, 1159–1163.
24 W. H. Baumann, M. Lehmann, A. Schwinde, R. Ehret, M. Brischwein and B. Wolf, *Sens. Actuator B-Chem.*, 1999, **55**, 77–89.
25 L. Berdondini, M. Chiappalone, P. D. van der Wal, K. Imfeld, N. F. de Rooij, M. Koudelka-Hep, M. Tedesco, S. Martinoia, J. van Pelt, G. Le Masson and A. Garenne, *Sens. Actuator B-Chem*, 2006, **114**, 530–541.
26 L. Griscom, P. Degenaar, B. LePioufle, E. Tamiya and H. Fujita, *Jpn. J. Appl. Phys. Part 1-Regul. Pap. Short Notes Rev. Pap.*, 2001, **40**, 5485–5490.
27 Y. Sugio, K. Komjima, H. Moriguchi, K. Takahashi and K. Yasuda, *Sens. Actuator B-Chem*, 2004, **99**, 156–162.
28 E. Claverol-Tinturé, M. Ghirardi, F. Fiumara, X. Rossel and J. Cabestany, *J. Neural Eng.*, 2005, **2**, L1–L7.
29 T. Kraus, E. Verpoorte, V. Linder, W. Franks, A. Hierlemann, F. Heer, S. Hafizovic, T. Fujii, N. F. de Rooij and S. Koster, *Lab Chip*, 2006, **6**, 218–229.
30 L. Rowe, M. Almasri, K. Lee, N. Fogleman, G. J. Brewer, Y. Nam, B. C. Wheeler, J. Vukasinovic, A. Glezer and A. B. Frazier, *Lab Chip*, 2007, **7**, 475–482.
31 B. J. Dworak and B. C. Wheeler, *Lab Chip*, 2009, **9**, 404–410.
32 L. Berdondini, P. Massobrio, M. Chiappalone, M. Tedesco, K. Imfeld, A. Maccione, M. Gandolfo, M. Koudelka-Hep and S. Martinoia, *J. Neurosci. Methods*, 2009, **177**, 386–396.
33 K. Imfeld, S. Neukom, A. Maccione, Y. Bornat, S. Martinoia, P. A. Farine, M. Koudelka-Hep and L. Berdondini, *IEEE Trans. Biomed. Eng.*, 2008, **55**, 2064–2073.
34 U. Frey, U. Egert, F. Heer, S. Hafizovic and A. Hierlemann, *Biosens Bioelectron.*, 2009, **24**, 2191–2198.
35 S. Hafizovic, F. Heer, T. Ugniwenko, U. Frey, A. Blau, C. Ziegler and A. Hierlemann, *J. Neurosci. Methods*, 2007, **164**, 93–106.
36 M. Hutzler, A. Lambacher, B. Eversmann, M. Jenkner, R. Thewes and P. Fromherz, *J. Neurophysiology*, 2006, **96**, 1638–1645.
37 M. Chiappalone, M. Bove, A. Vato, M. Tedesco and S. Martinoia, *Brain Res.*, 2006, **1093**, 41–53.
38 J. Van Pelt, P. S. Wolters, M. A. Corner, W. L. C. Rutten and G. J. A. Ramakers, *IEEE Trans. Biomed. Eng.*, 2004, **51**, 2051–2062.
39 Z. Chao, D. Bakkum, D. A. Wagenaar and S. Potter, *Neuroinformatics*, 2005, **3**, 263–280.
40 A. Gramowski, K. Jugelt, D. G. Weiss and G. W. Gross, *Eur. J. Neurosci.*, 2004, **19**, 2815–2825.
41 T. Opitz, A. D. De Lima and T. Voigt, *J. Neurophysiol.*, 2002, **88**, 2196–2206.
42 A. Araque, V. Parpura, R. P. Sanzgiri and P. G. Haydon, *Trends Neurosci.*, 1999, **22**, 208–215.
43 F. J. Diez-guerra and J. Avila, *Eur. J. Biochem.*, 1995, **227**, 68–77.
44 A. Maccione, M. Gandolfo, P. Massobrio, A. Novellino, S. Martinoia and M. Chiappalone, *J. Neurosci. Methods*, 2009, **177**, 241–249.
45 P. Bonifazi, M. E. Ruaro and V. Torre, *Eur. J. Neurosci.*, 2005, **22**, 2953–2964.
46 D. H. Perkel, G. L. Gerstein and G. P. Moore, *Biophys. J.*, 1967, **7**, 391–418.
47 S. G. Mallat, *IEEE T. Pattern Anal.*, 1989, **11**, 674–693.
48 M. Vetterli and C. Herley, *IEEE T. Signal. Process.*, 1992, **40**, 2207–2232.
49 K. Imfeld, A. Maccione, M. Gandolfo, S. Martinoia, P. A. Farine, M. Koudelka-Hep and L. Berdondini, *Int. J. Adapt. Control*, 2008, DOI: 10.1002/acs.1077.
50 S. Antic, G. Major and D. Zecevic, *J. Neurophysiol.*, 1999, **82**, 1615–1621.
51 G. C. Carlson and D. A. Coulter, *Nat. Protocols*, 2008, **3**, 249–255.